Use of Air-Liquid Two-Phase Flow in Hydrophobic Microfluidic Channels for Disposable Flow Cytometers

Dongeun Huh,[1] Yi-Chung Tung,[2] Hsien-Hung Wei,[1] James B. Grotberg,[1] Steven J. Skerlos,[2] Katsuo Kurabayashi,[2,3] and Shuichi Takayama[1,3]*

[1]Department of Biomedical Engineering, University of Michigan, Ann Arbor, 3304 GG Brown, 2350 Hayward, Ann Arbor, MI 48109-2125

[2]Department of Mechanical Engineering, University of Michigan, Ann Arbor, 2272 GG Brown, 2350 Hayward, Ann Arbor, MI 48109-2125

[3]Department of Macromolecular Science and Engineering, University of Michigan, Ann Arbor, Ann Arbor, MI 48109-2125
E-mail: Takayama@umich.edu

Abstract. This paper describes a disposable flow cytometer that uses an air-liquid two-phase microfluidic system to produce a focused high-speed liquid sample stream of particles and cells. The susceptibility of thin liquid columns to instabilities may suggest that focusing of sample liquids with streams of air would be difficult. The design of channel geometry, control of flow rates, and use of appropriate surface chemistries on the channel walls, however, enabled the generation of thin (15–100 µm) and partially bounded sample streams that were stable and suitable for rapid cell analysis. Using an inverted epi-fluorescence microscope with a photo-multiplier tube, we demonstrated that the system is capable of counting the number of beads and C_2C_{12} myoblast cells. The effects of different flow rates and surface chemistries of the channel walls on the air-liquid two-phase flows were characterized using optical and confocal microscopy. Use of air instead of liquids as a sheath fluid eliminates the need for large sheath liquid reservoirs, and reduces the volume and weight requirements. The low manufacturing cost and high volumetric efficiency make the air-sheath flow cytometer attractive for use as a stand-alone device or as an integrated component of bio-artificial hybrid microsystems.

Key Words. air sheath, flow cytometer, two-phase flow, surface chemistry, cell counting

Introduction

Flow cytometers use microfluidics and optics to detect and enumerate individual cells in a rapid manner (Shapiro, 1995). The instruments have gained widespread use in a variety of medical, scientific, and engineering fields such as disease diagnosis and monitoring (Stein et al., 1992; Fenili and Pirovano, 1998), cell biology (Harding et al., 2000), toxicology (Criswell et al., 1998), and environmental monitoring (Dubelaar and Gerritzen, 2000). Although conventional flow cytometers provide high-speed analytical capabilities, they are costly, bulky, and mechanically complex.

The growing need for less expensive and smaller instrumentation has motivated many efforts to reduce the cost and volume of both the fluidic and optical systems (Cunningham, 1990; Sobek et al., 1993; Niehren et al., 1995; Miyake et al., 1997; Cavender-Bares et al., 1998; Dubelaar et al., 1999; Fu et al., 1999; Harding et al., 2000; Miyake et al., 2000; Hung et al., 2001). Some research has demonstrated significant size and cost reduction of the optical system using solid-state lasers, sensors, and electronics (Zilmer et al., 1995; Dubelaar et al., 1999; Harding et al., 2000). Volume and cost reduction of the fluidic system, however, has been deterred by the requirement of a large amount of sheath liquid and the use of non-disposable fluidic modules. This paper describes the development of an air-liquid two-phase microfluidic system that enhances the portability and lowers the cost of flow cytometers.

Flow cytometers typically require 250–1,000 ml of aqueous sheath liquid to hydrodynamically focus 1 ml of biological sample. Previous works to miniaturize the fluidic system of flow cytometers have not addressed this need for large volumes of sheath liquid to process very small amount of sample suspension. Efforts have focused mainly on creating or modifying the design of surface/bulk micromachined sample focusing chambers and observation channels (Steen and Lindmo, 1979; Sobek et al., 1993; Miyake et al., 1997; Miyake et al., 2000; Hung et al., 2001). Moreover, microfluidic channels made out of silicon are complicated to fabricate, often requiring layer-by-layer bonding processes to give 3-dimensionality to the flow geometry and to incorporate glass substrates that provide an optical access for sample detection.

---

*Corresponding author.

Although there are systems that do not use sheath fluids (Crosland-Taylor, 1953; Fu et al., 1999), many of these systems have drawbacks such as channel clogging by sample particles or slow velocity of sample flow that decreases the optical detection rate (Crosland-Taylor, 1953). The current state-of-the-art for the fluidic systems of commercially available portable flow cytometers is to recycle the sheath liquid (Dubelaar and Gerritzen, 2000; Harding et al., 2000). These systems do reduce the need for large sheath liquid reservoirs, however, they are burdened by the requirement to have extra pumps and filters to recirculate the sheath fluid and remove particulates from the fluid. The use of air as a sheath fluid provides an alternative approach that opens new possibilities for the development of volume- and power-efficient systems. When ambient air is used as the sheath fluid, the supply is unlimited. The use of compressed gas as the source of sheath fluid would also be much more volume-efficient and may even be able to serve as the source of pressure to pump flows of gases and liquids. Moreover, the use of polymeric microfluidic channel provides disposable and optically transparent fluidic systems (Duffy et al., 1998) in which surface chemistries can be engineered to better control the air-liquid two-phase flows. In this paper, we demonstrate the feasibility of air-sheath-based flow cytometry by constructing a disposable air-liquid two-phase microfluidic system that can count cells and particles using an optical system based on an epi-fluorescence microscope equipped with a photo-multiplier tube (PMT) (Steen and Lindmo, 1979).

Design of the Air-Sheath Two-Phase Microfluidic System

The air-sheath flow cytometer has a simple polymeric microfluidic channel consisting of three flow compartments. Figure 1 shows the basic mechanism of the air sheath-driven flow. In the sample focusing chamber, the sample liquid is injected from the middle inlet port and is non-disruptively focused by air sheath flows coming in from the two side inlets. Downstream from the sample inlet, the chamber gradually constricts in order to induce a transitional acceleration until the two-phase flow reaches a high speed that enables rapid analysis of suspended particles and cells. The straight channel that follows has a constant width of 300 μm and forms the observation channel. In this region, the two-phase flow is maintained steadily along the length of the observation channel without any acceleration.

Experimental

The microfluidic channels of the air sheath-based flow cytometer were fabricated using soft lithography where poly(dimethylsiloxane) (PDMS) was cast against a silicon wafer mold having a 100 μm-thick SU-8 microfluidic channel feature prepared by photolithography (Duffy et al., 1998). The PDMS substrate with the channel feature embossed on one face was attached to a blank PDMS slab to produce a sealed fluidic system. In order to inject aqueous sample liquids in a controlled manner, a syringe pump was connected to the middle sample inlet port via a 16-gauge syringe needle and
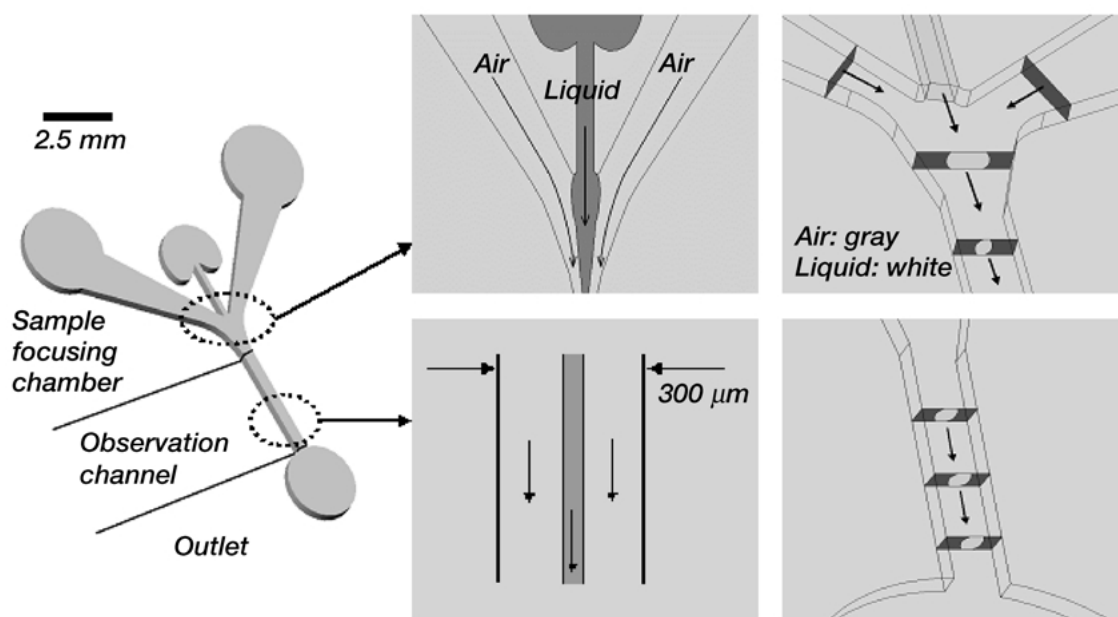

Fig. 1. Basic mechanism of aerodynamic focusing by air sheath flow. Undisturbed interaction of injected liquid flow with polymeric channel walls and air sheath flow produces a stable two-phase flow configuration throughout the flow cytometer channel. Channel height is 100 μm.

plastic tubing. Flow of air was driven by a vacuum pump connected to the outlet of the fluidic module. The microfluidic channel was placed on the stage of an epi-fluorescence microscope and images of the flow captured by a CCD camera (Orca-100, Hamamatsu Photonics, Japan). The effect of different flow rates on the sample stream was studied at a fixed vacuum pressure of 45 mmHg and the flow behavior of the air-water stratified flow was characterized by the shape of the resulting liquid column. A lower limit of the injection flow rate was determined by the onset of two-phase instabilities such as the break up of the column into droplets.

In order to assess the effect of surface chemistry, the cross-sections of two-phase flows were studied using confocal microscopy. Water containing fluorescein (Aldrich, St. Louis, MO) was injected into the microfluidic channel and the flow in the sample focusing chamber and observation channel was scanned by the blue laser illumination of a confocal microscope (LSM-510 confocal microscope, Zeiss, Germany).

Particle/cell detection was performed using a photo-multiplier tube (PMT) (P30CWAD5-01, Electron Tubes Inc., NJ) powered by a 900–1200 V voltage source and the detected fluorescence light signal was processed by a PC equipped with a data acquisition system (DAQ) (PCI-6111 DAQ card, National Instruments, TX). We performed counting of the number of red fluorescent particles (Spherotech, Inc., Libertyville, IL) having a size range of 15–19 μm in diameter. Particles suspended in water at a concentration of 0.0036% weight/volume were injected at 20 ml/hr and fluorescent emission from the excited beads in the sample core flow in the observation channel was detected at 5 MHz by the PMT and sampled at 50 kHz by the DAQ. We counted the number of freshly trypsinized C_2C_{12} myoblast cells suspended in phosphate buffered saline and labeled with Syto 9 (Molecular Probes, www.probes.com).

Results and Discussion

Generation of a stable flow of sample liquid is crucial for performing reliable flow cytometry and is the most critical technical issue for the development of the novel air-sheath-based microfluidic device. Focused air-liquid two-phase flows generated successfully inside hydro-phobic microfluidic channels are shown in Figure 2. Although the liquid column expands upon injection, it interacts stably with the air sheath flow and becomes constricted to a narrow stream along the center as the flow proceeds and enters the observation channel. Once in the observation channel, the width of the straight water column remains the same, which suggests that the flow is in the fully developed regime. The bulk velocity of the

water stream in this region was estimated by dividing the volumetric flow rate by the cross-sectional area of the water column to give rates of between 0.56–1.1 m/s. Under conditions of constant vacuum pressure, the width of the sample liquid column in the observation channel could be adjusted by changing the sample flow rate, where slower flow rates gave water streams with thinner widths (Figure 2). We maintained stable flows down to sample flow rates of 6 ml/hr, which yielded 15 μm wide water streams. Below this flow rate, the sample column no longer maintains its integrity and breaks up (Figure 2b). The ability to change the width of the sample liquid stream may be useful for accommodating differences in the size and concentration of the particles being analyzed.

Due to the large surface-area to volume ratios at the microscale, the properties of surfaces can have a profound influence on the behavior of fluids in microchannels (Zhao et al., 2001). To explore the effects of surface chemistry in the air-sheath flow cytometer, we fabricated a channel system that had the exact same geometry as the channel shown in Figure 2, but with hydrophilic channel walls instead of hydrophobic channel walls. In contrast to the stable aerodynamic focusing achieved in hydrophobic channels, hydrophilic channel walls cause the atomization of the water column in the sample focusing chamber and the lining of the spread water sample along the side walls of the observation channel (Figure 3). The cross-sectional views of the two-phase flow obtained by confocal microscopy (Figure 4) reveal the interaction between the channel wall and the aqueous stream for the different types of surface chemistry. These images help us understand the underlying mechanism of the surface chemistry-assisted aerodynamic focusing. In the hydro-phobic channel (Figure 4b), the air-water interface instantaneously forms a bulge after sample injection, and the water column becomes thin as the flow approaches the observation channel. The cross sectional images also tell us that the water column width is invariant along the observation channel suggesting that the flow is fully developed in that region. Flow in hydrophilic channels (Figure 4a), on the other hand, manifests totally different flow characteristics. A concave air-liquid interface is observed immediately after injection followed by the formation of a ''neck'' in the middle and rapid loss of its shape as the flow moves downstream of the sample focusing chamber. The sample stream then breaks up into small water droplets leading to atomization as the liquid enters the observation channel. Finally, selective build-up of the sample liquid around the corners was seen all along the length of the observation channel.

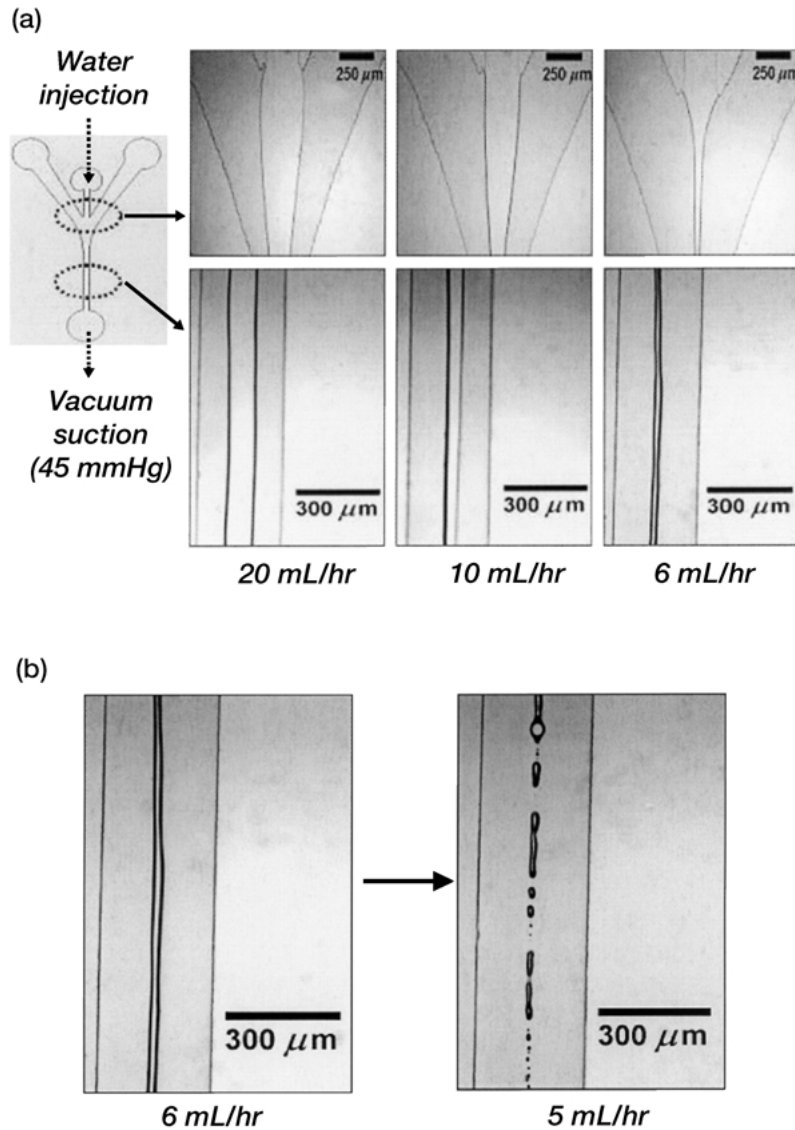The distinct flow behaviors of the water streams with

Fig. 2. (a) Stable aerodynamic focusing in the sample focusing chamber and stably maintained air-water two-phase straitifed flow in the observation channel. As the flow injection rate of the syringe pump is lowered, the width of the water column decreases. (b) Unstable flow behavior of water column observed under a critical flow rate from the syringe pump at which point the stream of water breaks up into droplets along the center of the observation channel.

different flow rates and properties of channel walls suggest that air-liquid two-phase stability in our fluidic system heavily depends on fluid dynamic conditions and surface chemistries. The relative importance between viscous, gravitational, and surface tension effects is estimated by the following two dimensionless parameters.

$$Ca_L = \frac{\mu_L U_L}{\sigma} \sim \frac{\text{viscous effect}}{\text{surface tension effect}}$$

$$Bo_L = \frac{\rho_L g d^2}{\sigma} \sim \frac{\text{gravitational effect}}{\text{surface tension effect}}$$

where μ_L is a viscosity of liquid, U_L is an average velocity of liquid flow, σ is a surface tension between air and liquid, ρ_L is the density of liquid, g is the gravitational acceleration, and d is the channel height. Assuming that the channel wall is likely to be somewhat contaminated during the fabrication process of the fluidic module, σ was estimated to have a value of 30 dynes/cm, which is a typical magnitude of surface tension between air and water on a contaminated polymeric surface. It was shown that $Bo_L = 3 \times 10^{-3}$. This small number indicates that in the air-sheath fluidic system, gravity has a negligible influence on the flow compared to surface
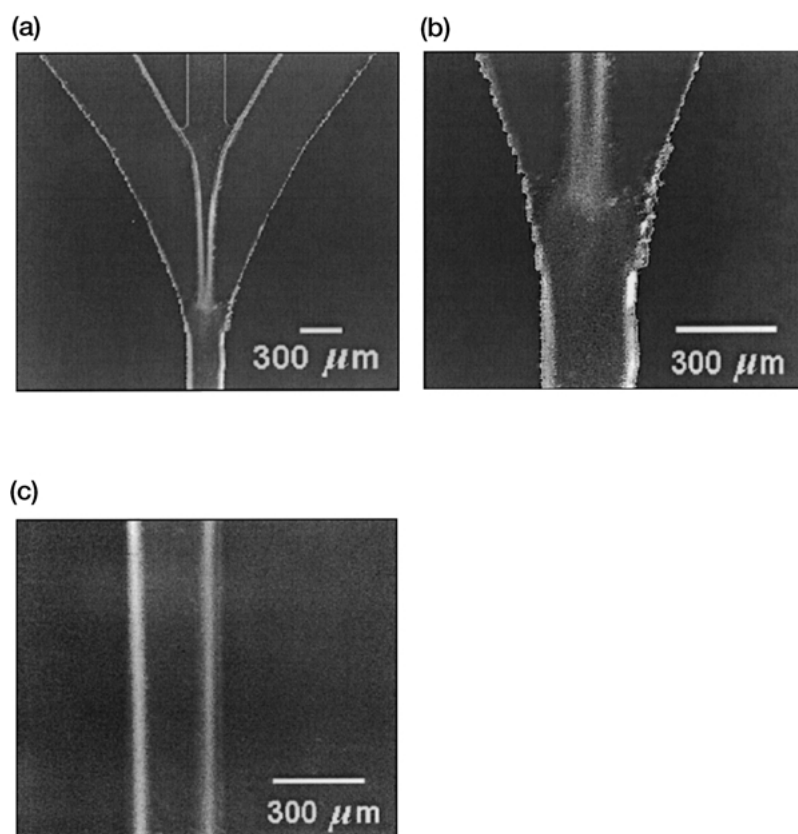
Fig. 3. *Air-liquid two-phase flow in a hydrophilic channel. (a)(b) In the sample focusing chamber, water column atomizes and forms spray of small water droplets. (c) In the observation channel, the aqueous sample liquid flows along the channel side-walls, and is observed as thick white lines along the length of the observation channel.*

tension effects. For average velocities (U_L) determined by dividing tested liquid flow rates (6–20 ml/hr) by the cross sectional area of the injection nozzle $(250\,\mu m \times 100\,\mu m = 2.5 \times 10^4\,\mu m^2)$, the Ca_L was calculated to be on the order of $10^{-3}(2.2 \times 10^{-3} - 7.3 \times 10^{-3})$ and similarly, the small value tells us that surface tension dominates over viscous force. The fact that the two-phase microfluidic system is dominated by surface tension permits the interpretation of different flow behaviors of liquid flow in terms of the relative surface affinity of the PDMS channel wall for water. The high affinity of the hydrophilic channel wall pulls the water column towards the top and bottom channel walls, splitting the column at the ''neck'' region. The build-up of the sample stream around the corners of the channel is attributed to the thermodynamic behavior of the two-phase system to minimize interfacial surface area, thus achieving a lower energy state. Instead of forming thin aqueous layers at the top and bottom walls, the surface area of the phase interface is minimized by redistribution of liquid into the corners. In the hydrophobic channel, the water stream is repelled by the top and bottom wall surfaces due to their low affinity for water, which assists in maintaining the column structure without spreading. In addition, the hydrophobicity of the channel walls discourages lateral movement of the water column by effectively ''pinning'' the liquid column at the four interface-wall contact lines. The pinning occurs because there is no energetic incentive for the aqueous solution to move laterally due to the low affinity of the channel for water, which makes it necessary to have additional forces for movement of the aqueous sample stream.

Furthermore, in the normal stress boundary condition that determines the interfacial shape under dynamic two-phase flow environments, the viscous force term is negligible and the equation reduces to the Young-Laplace equation, which dictates the shape of *static* air-liquid interfaces. That is, the contact angle between the water column and the hydrophobic channel wall is the same as the static contact angle even in the presence of high-velocity air and water flow in the longitudinal direction. It is noted that the top and bottom do not have the same contact angle. This is a result of the molding
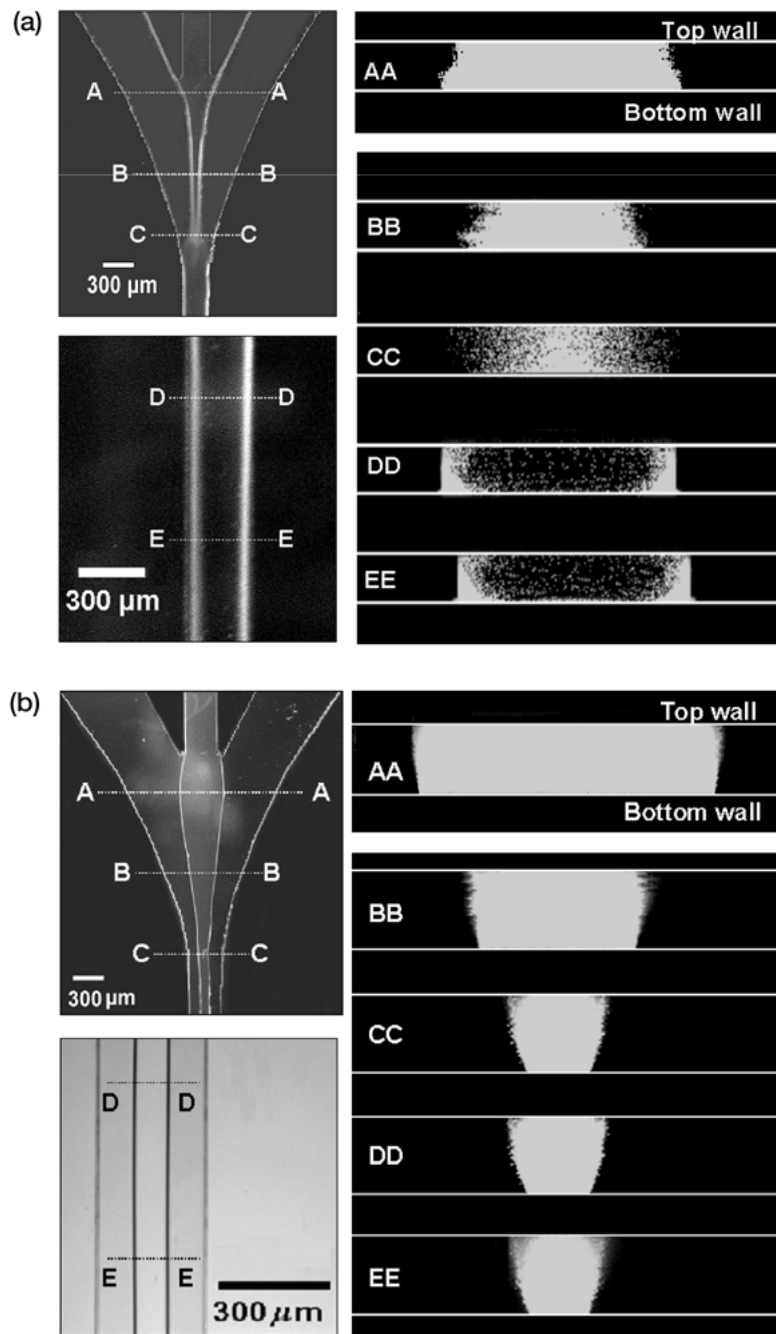
Fig. 4. *Cross sectional images of liquid column in (a) a hydrophilic channel and (b) hydrophobic PDMS channel. Water containing fluorescein was used as a sample liquid in confocal microscope imaging.*

processes. The top wall was replicated from an SU-8 on silicon mold, whereas the bottom wall was a flat slab of PDMS cast in a petridish. By measuring sessile contact angles of water on PDMS surfaces prepared by casting against an SU-8 resist (94.47°) or a petridish (108.56°), it was experimentally confirmed that the contact angle of water on PDMS differs depending on the molding pro-

cedures. These values agree well with the contact angles measured in the cross sectional confocal image of the water column in the hydrophobic observation channel.

To characterize fluid dynamic conditions for stable aerodynamic focusing in hydrophobic channels, we used *Re* of liquid flow in the upstream region of the sample focusing chamber, which is given by

$$Re_{L,\text{up}} = \frac{U_{L,\text{up}}d}{\nu_L} = \frac{Q_L d}{A_L \nu_L}$$

$$= \frac{(\text{flow rate of sample liquid}) \times (\text{channel height})}{(\text{area of injection nozzle}) \times (\text{kinematic viscosity of liquid})}.$$

Considering that the surface area of the liquid sample injection nozzle is $250\,\mu m \times 100\,\mu m = 2.5 \times 10^4\,\mu m^2$, the minimum flow rate (6 ml/hr) required to achieve a stable liquid stream yields a $Re_{L,\text{up}} = 6.6$ and below this limit, the flow becomes unstable and eventually breaks up. On the other hand, if the flow rate is larger than 50 ml/hr, the channel is filled with sample liquid even in the presence of vacuum suction at the outlet. This indicates that there is an upper limit of $Re_{L,\text{up}}(= 55.5)$ that causes fill-up of the channel with the liquid stream. Consequently, for a fixed vacuum pressure, there is a range of $Re_{L,\text{up}}$ in which the liquid stream is stably maintained.

In order to estimate the *Re* of the air and water streams in the observation channel, $(Re_{L,\text{down}}$ and $Re_{a,\text{down}})$, the stable two-phase flow in the observation channel was mathematically modeled under the following assumptions: (i) Fluid is Newtonian and incompressible. (ii) Flow is fully developed in the *x*-direction (flow direction) and thus, flow has no *x*-dependence. (iii) Gas-liquid interface is flat, and the axial pressure gradient in liquid and gas flows are the same. Since the flow field seen from the top is symmetric with respect to $x = 0$, only half of the whole flow was considered in the modeling (Figure 5a) (see notes for more details). Figure 5b shows an example of a velocity field for the flow configuration
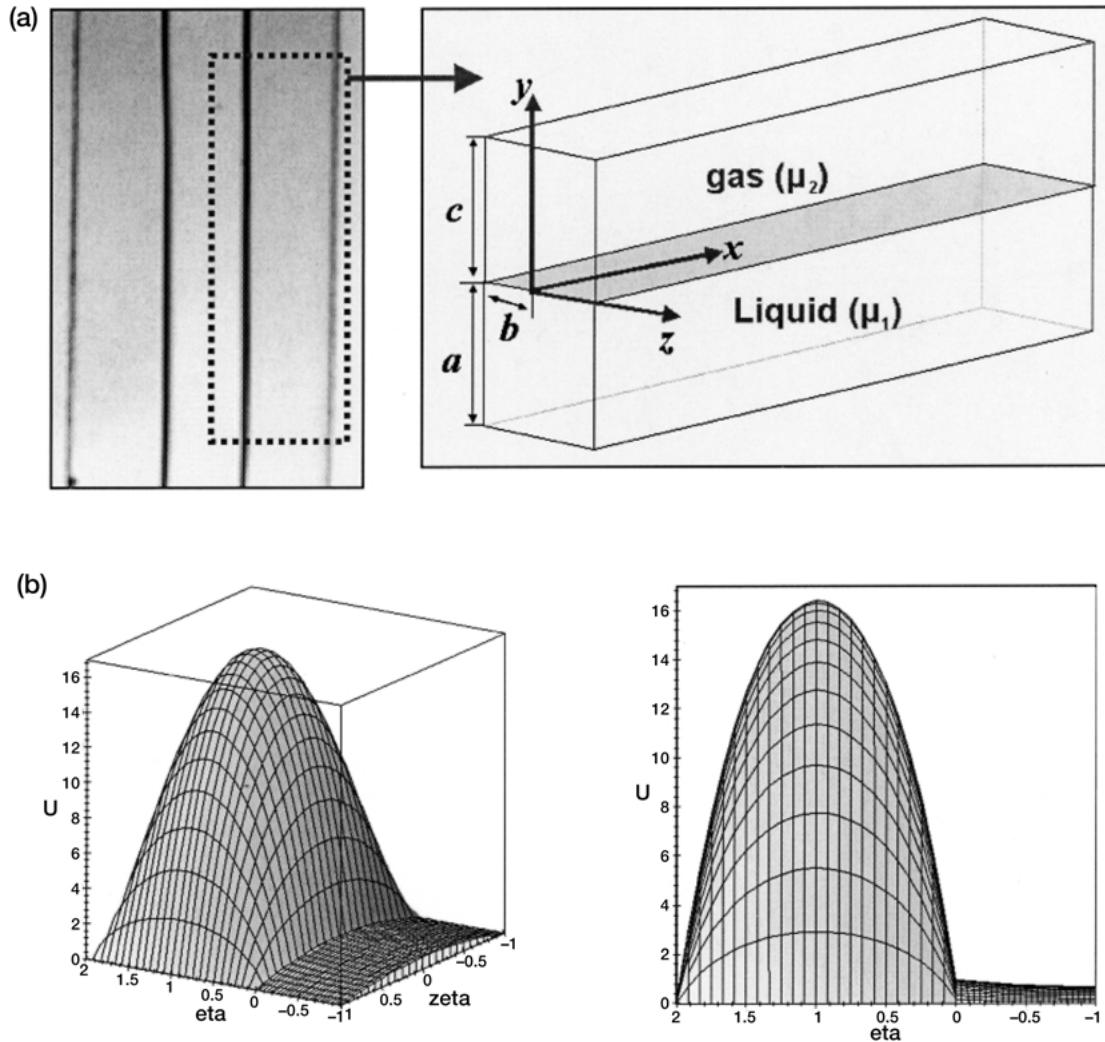

Fig. 5. *(a) Flow geometry for mathematical model of gas-liquid two-phase flow in the observation channel. Only half of the whole flow field is shown here. Flow proceeds in the positive x-direction and the plane of y = 0 represents a flat gas-liquid interface. Geometrical constraints are given by a + c = 150 μm and 2b = 100 μm. (b) Velocity distribution of air-water two phase flow ($\beta = \mu_1/\mu_2 = 55$ (water/air), $\lambda = b/a = 50\,\mu m/50\,\mu m = 1$, and $\gamma = c/a = 100\,\mu m/50\,\mu m = 2$). Eta and zeta axes represent dimensionless y and z position, respectively. U is a dimensionless x-directional velocity. See notes for details.*

achieved at a liquid volumetric flow rate (Q_L) of 20 ml/ hr. As seen in the plot, air-sheath flow travels much faster than the liquid stream mainly due to its smaller viscosity. In this case, our mathematical model predicts the flow rate of air to be $Q_a = 45Q_L = 900$ ml/hr, and the corresponding *Re* of the air and liquid flows given by

$$Re_{a,\text{down}} = \frac{U_{a,\text{down}}d}{\nu_a} = \frac{Q_a d}{A_a \nu_a}$$
$$= \frac{(\text{flow rate of air flow}) \times (\text{channel height})}{(\text{cross section of air flow}) \times (\text{kinematic viscotiy of air})}$$
$$Re_{L,\text{down}} = \frac{U_{L,\text{down}}d}{\nu_L} = \frac{Q_L d}{A_L \nu_L}$$
$$= \frac{(\text{flow rate of liquid flow}) \times (\text{channel height})}{(\text{cross section of liquid flow}) \times (\text{kinematic viscotiy of liquid})}$$

are 83.3 and 55.6, respectively. At a lower limit of liquid flow rate $(Q_L = 6$ ml/hr$)$, the theoretical prediction yields $Q_a = 128Q_L = 768$ ml/hr,   which   gives $Re_{a,\text{down}} = 49.9$ and $Re_{a,\text{down}} = 111.1$.

Finally, the particle/cell detection capability of the two-phase microfluidic system was demonstrated using an epi-fluorescence microscope mounted with a PMT (Steen and Lindmo, 1979). The light intensity of the signal output emitted from red fluorescent particles was plotted with respect to time. The detection was conducted for 3 seconds, and the noise signals generated by dark background were sorted out by establishing a signal threshold when measuring the signal peaks. The flux of the fluorescent beads passing though the detection spot of the observation channel was theoretically predicted to be 55–113 beads/sec for a volumetric flow rate of 20 ml/hr, based on the given concentration and size distribution of the suspended particles (15–19 µm). The mean of 9 counting experiments was 87 beads/sec and closely matched the predicted number of beads per second. The operation of the system was also confirmed by measuring the number of suspended C_2C_{12} myoblast cells. The number of cells evaluated by the experiment was 100 cells/sec.

Conclusion

We have demonstrated the use of air-liquid two-phase flows in polymeric channels to achieve a space-saving and disposable flow cytometry system that can analyze cells and particles. Although the system still has a lower performance compared to that of conventional flow cytometers and its choice of sample fluids is currently limited to solutions that do not contain surface-wetting materials (e.g. amphiphiles, surfactants), the air sheath mechanism opens new opportunities and provides some capabilities that are more advantageous or complemen-

tary to conventional instruments: (i) Elimination of sheath liquid and use of disposable microchannels lowers the cost and size requirements making the air-sheath flow cytometer attractive for the development of portable biological sample analysis devices, multiplexed parallel analysis systems, and integrated bio-artificial hybrid microsystems. (ii) The elimination of the sheath liquid also prevents the sample suspension from being diluted by sheath liquids. This may be important for analyzing samples that one needs to recover after analysis. (iii) The sensitivity of the sample liquid flow to surface properties opens the possibility of using thermal (Kataoka and Troian, 1999) or electrowetting (Pollack et al., 2000) mechanisms to produce movement of liquid columns for cell and particle sorting. This type of fluid actuation is not possible in single-phase flows used by conventional flow cytometers. (iv) The two-phase system provides a gas-liquid interface that may also be useful for analysis of gasses (Zhao et al., 2001) or airborne chemicals and particles.

Partially bounded air-liquid two-phase flows in microfluidic systems are not only of practical significance for reliable flow cytometric instrumentation, but also presents an interesting fundamental phenomenon in fluid mechanics. Based on experimental observations of sample stream at different volumetric flow rates, we performed a dimensional analysis to characterize the flow system. We found that for a given pressure difference between the air inlet and outlet, there are critical values of Re_L (liquid Reynolds number) that achieve a stable liquid stream. We are currently exploring further theoretical and experimental analysis of the two-phase microfluidic system as well as developing microscale integrated systems that use the air-sheath flow cytometers as a component of a total cell culture/ analysis system.

Appendix

Dimensionless momentum equations for fully developed flow in the *x*-direction are

$$\lambda^2 u_{1\eta\eta} + u_{1\zeta\zeta} = -1$$
$$\lambda^2 u_{2\eta\eta} + u_{2\zeta\zeta} = -\beta, \text{ where } \beta = \mu_1/\mu_2$$

where $\mu_1 =$ liquid   viscosity, $\mu_2 =$ gas   viscosity, $\beta = \mu_1/\mu_2$, $u = u^*/(Gb^2/\mu_1)$, $\eta = y/a$, $\zeta = z/b$, $\lambda = b/a$, $G =$ constant axial pressure gradient. Subscripts 1 and 2 represent liquid and gas phase, respectively. Boundary conditions are given by

$u_1(\zeta = \pm 1) = 0$, $u_2(\zeta = \pm 1) = 0$, $u_2(\eta = c/a = \gamma) = 0$
(no slip condition at the channel walls)

$u_1(\eta = 0) = u_2(\eta = 0)$,   (velocity matching at the interface)

$\beta \dfrac{\partial u_1}{\partial \eta}\bigg|_{\eta = 0} = \dfrac{\partial u_2}{\partial \eta}\bigg|_{\eta = 0}$,   (shear stress matching at the interface)

$\dfrac{\partial u_1}{\partial \eta}\bigg|_{\eta = -1} = 0$ (symmetry at the mid plane)

Particular solutions to the nonhomogeneous partial differential governing equations which satisfy the no slip boundary condition at $\zeta = \pm 1$ are

$$u_{1p}(\zeta) = \frac{1}{2}(1 - \zeta^2), \ u_{2p}(\zeta) = \frac{\beta}{2}(1 - \zeta^2).$$

On the other hand, homogeneous solutions can be expressed as Fourier series expansions that satisfy the no slip condition at $\zeta = \pm 1$.

$$u_{1h}(\eta, \zeta) = \sum_{n=1}^{\infty} A_{1n}(\eta)\cos(k_n\zeta),$$
$$u_{2h}(\eta, \zeta)$$
$$= \sum_{n=1}^{\infty} A_{21n}(\eta)\cos(k_n\zeta)$$

where $k_n = (2n + 1)\pi/2$. Substitution of the solutions into the homogeneous governing equations yields two ordinary differential equations necessary to determine the unknown functions $A_{1n}(\eta)$ and $A_{2n}(\eta)$.

$$\lambda^2 A_{1n}'' + k_n^2 A_{1n} = 0$$
$$\lambda^2 A_{2n}'' + k_n^2 A_{2n} = 0.$$

Expressing the particular solutions u_{1p} and u_{2p} as Fourier series expansions, the total solutions for u are written as

$$u_1(\eta, \zeta) = \sum_{n=0}^{\infty} \bigg[f_{1n}$$
$$+ C_{1n}\cosh\left(\frac{k_n}{\lambda}\eta\right) + C_{2n}\sinh\left(\frac{k_n}{\lambda}\eta\right) \bigg]\cos(k_n\zeta)$$
$$u_2(\eta, \zeta) = \sum_{n=0}^{\infty} \bigg[\beta f_{1n} + C_{3n}\cosh\left(\frac{k_n}{\lambda}\eta\right)$$
$$+ C_{4n}\sinh\left(\frac{k_n}{\lambda}\eta\right)\bigg]\cos(k_n\zeta)$$

where $f_{1n} = 16(-1)^n/((2n+1)^3\pi^3)$ and the unknown coefficients $(C_{1n}, C_{2n}, C_{3n}, C_{4n})$ can be determined from boundary conditions. Figure 5b shows an example velocity field for $\beta = \mu_1/\mu_2 = 55$ (water/air), $\lambda = b/a = 50\,\mu m/50\,\mu m = 1$, and $\gamma = c/a = 100\,\mu m/$ 50 μm = 2, the flow configuration achieved at a liquid volumetric flow rate (Q_L) of 20 ml/hr.

Acknowledgments

References

K.K. Cavender-Bares, S.L. Frankel, and S.W. Chisholm, Limnol. Oceanography **43**(6), 1383–1388 (1998).

K.A. Criswell, M.R. Bleavins, D. Zielinski, J.C. Zandee, and K.M. Walsh, Cytometry **32**(1), 18–27 (1998).

P.J. Crosland-Taylor, Nature **171**, 37–38 (1953).

A. Cunningham, J. Plankton Res. **12**(1), 149–160 (1990).

G.B.J. Dubelaar and P.L. Gerritzen, Scientia Marina **64**(2), 255–265 (2000).

G.B.J. Dubelaar, P.L. Gerritzen, A.E.R. Beeker, R.R. Jonker, and K. Tangen, Cytometry **37**(4), 247–254 (1999).

D.C. Duffy, J.C. McDonald, O.J.A. Schueller, and G.M. Whitesides, Anal. Chem. **70**(23), 4974–4984 (1998).

D. Fenili and B. Pirovano, Clin. Chem. Lab. Med. **36**(12), 909–917 (1998).

A.Y. Fu, C. Spence, A. Scherer, F.H. Arnold, and S.R. Quake, Nature Biotech. **17**(11), 1109–1111 (1999).

C.L. Harding, D.R. Lloyd, C.M. McFarlane, and M. Al-Rubeai, Biotechnol. Prog. **16**(5), 800–802 (2000).

C.I. Hung, B.J. Ke, G.R. Huang, B.H. Hwei, H.F. Lai, and G.B. Lee, J. Fluids Eng.-Trans. Asme **123**(3), 672–679 (2001).

D.E. Kataoka and S.M. Troian, Nature **402**(6763), 794–797 (1999).

R. Miyake, H. Ohki, I. Yamazaki, and T. Takagi, Jsme Int. J. B—Fluids Thermal Eng. **40**(1), 106–113 (1997).

R. Miyake, H. Ohki, I. Yamazaki, and T. Takagi, Jsme Int. J. B-Fluids Thermal Eng. **43**(2), 219–224 (2000).

S. Niehren, W. Kinzelbach, S. Seeger, and J. Wolfrum, Anal. Chem. **67**(15), 2666–2671 (1995).

M.G. Pollack, R.B. Fair, and A.D. Shenderov, Appl. Phys. Lett. **77**(11), 1725–1726 (2000).

H.M. Shaprio, *Practical flow cytometry* (Wiley-Liss, New York, 1995).

D. Sobek, A.M. Young, M.L. Gray, and S.D. Senturia, Proc. IEEE **2**, 219–224 (1993).

H.B. Steen and T. Lindmo, Science **204**, 403–404 (1979).

D.S. Stein, J.A. Korvick, and S.H. Vermund, J. Infect. Dis. **165**(2), 352–363 (1992).

B. Zhao, J.S. Moore, and D.J. Beebe, Science **291**(5506), 1023–1026 (2001).

N.A. Zilmer, M. Godavarti, J.J. Rodriguez, T.A. Yopp, G.M. Lambert, and D.W. Galbraith, Cytometry **20**(2), 102–117 (1995).